Supporting Information for

Long-Range Observation of Exciplex Formation and Decay Mediated by One-Dimensional Bridges

Jinseok Baek,[†] Tomokazu Umeyama,*[,†] Kati Stranius,[§] Hiroki Yamada,[†] Nikolai V. Tkachenko,*[,§] and Hiroshi Imahori*[,†,‡]

[†]*Department of Molecular Engineering, Graduate School of Engineering, Kyoto University, Nishikyo-ku, Kyoto 615-8510, Japan*

[§]*Laboratory of Chemistry and Bioengineering, Tampere University of Technology, P.O. Box 541, FIN-33101 Tampere, Finland*

[‡]*Institute for Integrated Cell-Material Sciences (WPI-iCeMS), Kyoto University, Sakyo-ku, Kyoto 606-8501, Japan*

E-mail : umeyama@scl.kyoto-u.ac.jp, nikolai.tkachenko@tut.fi, imahori@scl.kyoto-u.ac.jp

Experimental

Materials. All solvents and chemicals were of reagent grade quality, purchased, and used without further purification. 5-(Pinacolatoboryl)-10,15,20-tris(3,5-di-*tert*-butylphenyl)-porphyrinatozinc(II) (ZnP-Bpin),[S1] 5-bromo-10,15,20-tris(3,5-di-*tert*-butylphenyl)-porphyrinatozinc(II) (ZnP-ph_0-Br),[S2] 5,10,15,20-tetra(3,5-di-*tert*-butylphenyl)-porphyrinatozinc(II) (ZnP-ref),[S1] 4,4'-dibromo-2,2',5,5'-tetramethyl-1,1'-biphenyl (Br-xy_2-Br),[S3] and 4,4''-dibromo-2,2',2'',5,5',5''-hexamethyl-1,1':4',1''-terphenyl (Br-xy_3-Br)[S4] were prepared according to the reported procedures.

Synthesis

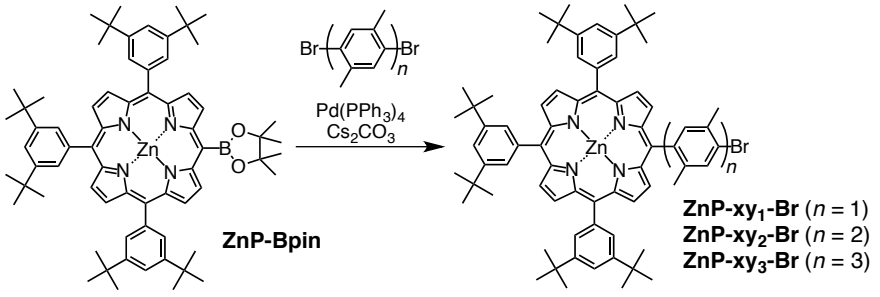

Synthesis of ZnP-xy_1-Br. ZnP-Bpin (213 mg, 0.2 mmol), 1,4-dibromo-2,5-dimethylbenzene (211 mg, 0.8 mmol), $Pd(PPh_3)_4$ (24 mg, 0.02 mmol) and Cs_2CO_3 (260 mg, 0.8 mmol) were dried under vacuum and then purged with argon. To this mixture degassed toluene (15 mL) was added and stirred for 24 hours at 96 °C. After cooling, water (200 mL) was added and extracted organic layer with CH_2Cl_2 and dried over anhydrous Na_2SO_4. The solvent was evaporated the residue was purified by column chromatography (silica gel, $CHCl_3$: hexane = 3:7) to give the product as a dark purple solid (85% yield, 194 mg, 0.174 mmol). Melting point: > 300 °C. ^{1}H NMR (400 MHz, $CDCl_3$) δ 9.01-8.98 (m, 6H), 8.83 (d, J = 4 Hz, 2H), 8.13 (t, J = 8.4 Hz, 7H), 7.91 (s, 1H), 7.80 (s, 3H), 2.59 (s, 3H), 2.05 (s, 3H), 1.54 (s, 54H). ^{13}C NMR ($CDCl_3$, 75.45 MHz), δ: 150.5, 150.4, 149.6,

148.6, 141.8, 138.9, 136.1, 133.2, 132.6, 132.5, 132.3, 132.2, 130.9, 129.8, 129.6, 124.4, 122.7, 122.4, 120.8, 118.1, 35.1, 31.8, 22.5, 20.7. IR (ATR): 3053, 2952, 2866, 1590, 1474, 1392, 1361, 1289, 1246, 1218, 1053, 1002, 931, 899, 879, 823, 797, 753, 716, 440 cm^{-1}. HRMS (ESI+, m/z) = 1118.4748; calcd for $C_{70}H_{79}BrN_4Zn$: 1118.4780.

Synthesis of ZnP-xy$_2$-Br. This compound was prepared from Br-xy$_2$-Br by the identical procedure of ZnP-xy$_1$-Br (76% yield). Melting point: > 300 °C. ^{1}H NMR (300 MHz, $CDCl_3$) δ 9.04-8.99 (m, 7H), 8.89-8.85 (m, 1H), 8.18-8.10 (m, 6H), 7.96 (d, J = 6 Hz, 1H), 7.83 (s, 3H), 7.62 (s, 1H), 7.40 (s, 1H), 7.34 (s, 1H), 2.55 (s, 3H), 2.38 (s, 3H), 2.27 (s, 3H), 2.11 (s, 3H), 1.55 (s, 54H). ^{13}C NMR ($CDCl_3$, 75.45 MHz), δ: 150.5, 150.4, 150.0, 149.7, 148.6, 148.5, 141.9, 141.8, 141.5, 141.1, 140.3, 138.9, 136.7, 135.6, 134.9, 133.4, 133.2, 132.6, 132.5, 132.3, 132.2, 132.1, 131.9, 131.3, 131.1, 130.9, 129.9, 129.8, 129.7, 129.6, 129.5, 124.5, 124.4, 123.4, 122.5, 122.4, 122.3, 120.8, 120.7, 119.6, 117.8, 35.1, 31.9, 31.8, 31.7, 22.5, 20.9, 19.7, 19.3. IR (ATR): 3052, 2954, 2920, 2851, 1591, 1460, 1392, 1362, 1339, 1288, 1247, 1219, 1070, 1047, 1003, 932, 898, 882, 824, 799, 763, 740, 717, 635, 616, 535, 460, 411 cm^{-1}. HRMS (ESI+, m/z) = 1222.5385; calcd for $C_{78}H_{87}BrN_4Zn$: 1222.5406.

Synthesis of ZnP-xy$_3$-Br. This compound was prepared from Br-xy$_3$-Br by the identical procedure of ZnP-xy$_1$-Br (64% yield). Melting point: > 300 °C; ^{1}H NMR (300 MHz, $CDCl_3$) δ 9.03-8.98 (m, 7H), 8,89 (d, J = 4.8 Hz, 1H), 8.15-8.08 (m, 6H), 7.94 (s, 1H), 7.80 (s, 3H), 7.51 (s, 1H), 7.41 (s, 1H), 7.38 (d, J = 3.7 Hz, 1H), 7.16 (s, 1H) 7.11 (d, J = 3.3 Hz, 1H), 2.45 (s, 3H), 2.38 (s, 3H), 2.18-2.15 (m, 6H), 2.10 (s, 3H), 1.54 (s, 54H). ^{13}C NMR ($CDCl_3$, 75.45 MHz), δ: 150.7, 150.3, 148.8, 141.2, 135.8, 133.5, 132.6, 132.4, 132.3, 131.3, 130.8, 130.0, 129.9, 129.8, 122.7, 122.4, 121.0, 120.0, 35.1, 31.8, 23.9, 22.4, 21.0, 19.6, 19.4. IR (ATR): 3051, 2952, 2860, 1657, 1590,

1476, 1424, 1391, 1361, 1339, 1287, 1246, 1218, 1050, 1001, 932, 881, 823, 797, 715, 667, 547, 455, 430, 412 cm^{-1}. HRMS (ESI+, m/z) = 1326.6020; calcd for $C_{86}H_{95}BrN_4Zn$: 1326.6032.

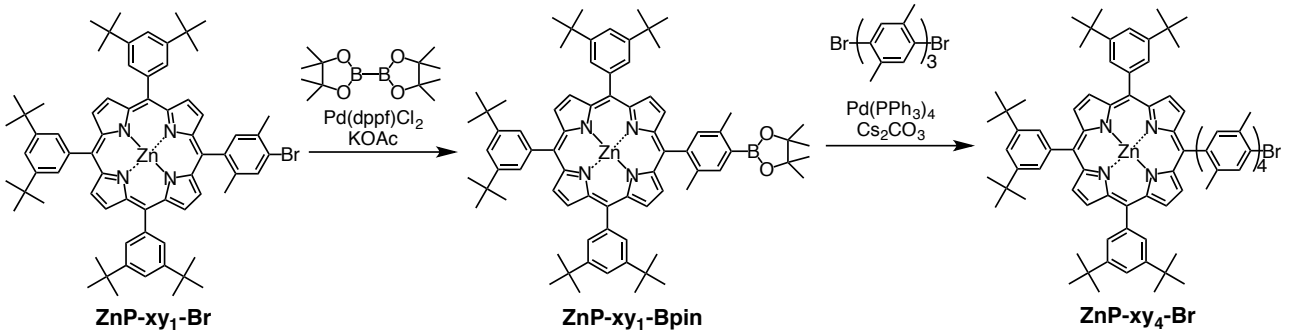

Synthesis of ZnP-xy$_1$-Bpin. A 50 mL Schlenk flask was charged with ZnP-xy$_1$-Br (223 mg, 0.2 mmol), bis(pinacolato)diborone (200 mg, 0.8 mmol), potassium acetate (KOAc) (60 mg, 0.6 mmol), Pd(dppf)Cl_2 (15 mg, 0.02 mmol) and dehydrated toluene (25 mL) under argon. This mixture was then degassed via three cycles of freeze-pump-thaw and refilled with argon. The reaction mixture was stirred for 24 hours at 105 °C. After cooling, water was added and extracted organic layer with CH_2Cl_2 and dried over anhydrous Na_2SO_4. After removal of the solvent, the crude product was purified by column chromatography (silica gel, CH_2Cl_2:hexane = 1:2) to give the dark purple solid product (60% yield, 140 mg, 0.12 mmol). Melting point: > 300 °C; ^{1}H NMR (300 MHz, $CDCl_3$) δ 9.02 (d, J = 4.5 Hz, 2H), 8.99 (d, J = 4.4 Hz, 2H), 8.14-8.09 (m, 6H), 8.02 (s, 1H), 7.88 (s, 1H), 7.81 (s, 3H), 2.51 (s, 3H), 2.09 (s, 3H), 1.56 (s, 54H), 1.36 (s, 12H). ^{13}C NMR ($CDCl_3$, 75.45 MHz), δ: 150.6, 150.5, 150.4, 149.9, 148.6, 145.1, 142.0, 141.8, 140.2, 136.5, 135.9, 134.0, 132.5, 132.2, 132.1, 131.6, 131.3, 129.9, 129.7, 122.3, 120.8, 119,8, 83,7, 83.4, 35.0, 31.7, 25.0, 21.7, 20.7. IR (ATR): 2960, 2866, 1591, 1462, 1392, 1366, 1341, 1305, 1263, 1215, 1143, 1070, 1003, 904, 855, 822, 799, 756, 732, 681, 665, 580, 516, 416 cm^{-1}. HRMS (ESI+, m/z) = 1166.6495; calcd for $C_{76}H_{91}BN_4O_2Zn$: 1166.6527.

Synthesis of ZnP-xy$_4$-Br. ZnP-xy$_1$-Bpin (140 mg, 0.12 mmol), Br-xy$_3$-Br (226 mg, 0.48 mmol), $Pd(PPh_3)_4$ (14 mg, 0.012 mmol) and Cs_2CO_3 (157 mg, 0.48 mmol) were dried under vacuum and then purged with argon. To this mixture degassed toluene (15 mL) was added and stirred for 24 hours at 105 °C. After cooling, water (200 mL) was added and extracted organic layer with CH_2Cl_2 and dried over anhydrous Na_2SO_4. The solvent was evaporated, and the residue was purified by column chromatography (silica gel, DCM: hexane = 1:2) to give the product as a dark purple solid (60% yield, 103 mg, 0.072 mmol). Melting point: > 300 °C; ^{1}H NMR (400 MHz, $(CD_3)_2CO$) δ 8.91-8.85 (m, 8H), 8.16 (s, 2H), 8.11 (s, 4H), 8.00 (s, 1H), 7.94 (s, 3H), 7.55 (s, 1H), 7.46 (d, J = 9.8 Hz, 2H), 7.23 (s, 1H), 7.18 (d, J = 8 Hz, 2H), 7.08 (s, 1H), 2.78 (s, 18H), 2.44 (s, 3H), 2.37 (s, 3H), 1.57 (s, 54H). ^{13}C NMR ($CDCl_3$, 75.45 MHz), δ: 150.4, 150.3, 150.1, 148.5, 141.9, 136.4, 135.5, 133.2, 133.0, 132.9, 132.4, 132.1, 131.9, 131.8, 131.3, 130.9, 130.5, 129.9, 129.7, 129.5, 129.0, 128.2, 125.3, 122.5, 122.3, 120.8, 120.7, 120.0, 35.1, 31.8, 22.3, 21.4, 21.0, 19.4. IR (ATR): 2955, 2862, 1591, 1476, 1392, 1362, 1289, 1258, 1219, 1023, 931, 881, 797, 715, 471, 455, 411 cm^{-1}. HRMS (ESI+, m/z) = 1430.6623; calcd for $C_{94}H_{103}BrN_4Zn$: 1430.6658.

Photoelectrochemical Measurements. All photoelectrochemical measurements were carried out in a standard three-electrode system using an ALS 630A electrochemical analyzer. The deposited film as a working electrode was immersed into an electrolyte solution containing 0.5 M LiI and 0.01 M I_2 in acetonitrile. A Pt wire covered with a glass Luggin capillary, whose tip was located near the working electrode, was used as a quasi-reference electrode. A Pt coil was employed as a counter electrode. The potential measured was converted to the saturated calomel electrode (SCE) scale by adding +0.05 V. A 500 W xenon lamp (XB-50101AAA; USHIO, Japan) was used as a light source. White light (λ > 380 nm; input power, 35 mW cm^{-2}) or monochromatic light through a

monochromator (MC-10N; Ritsu, Japan) was illuminated on the modified area of the working electrode (0.20 cm^2) from the backside. The light intensity was monitored by an optical power meter (ML9002A; Anritsu, Japan) and corrected for calculation of IPCE values.

Table S1. Edge-to-edge separation distance between ZnP and SWNTs (R_{DA}), fluorescence lifetimes (τ_S), rate constant for exciplex formation (k_{FEX}), lifetimes of the fourth component in TA (τ_4) and rate constant for exciplex decay (k_{DEX}) of ZnP-xy$_{n-1}$-ph$_1$-SWNT (n = 1–5).

n	R_{DA} / Å	τ_S / ps	k_{FEX} / s^{-1}	τ_4 / ps	k_{DEX} / s^{-1}
1	5.8	8.0	1.25×10^{11}	236	4.24×10^{9}
2	10.1	13.2	7.53×10^{10}	500	2.00×10^{9}
3	14.5	21.7	4.56×10^{10}	875	1.14×10^{9}
4	18.3	34.0	2.89×10^{10}	1457	6.86×10^{8}
5	22.6	59.0	1.65×10^{10}	2710	3.69×10^{8}

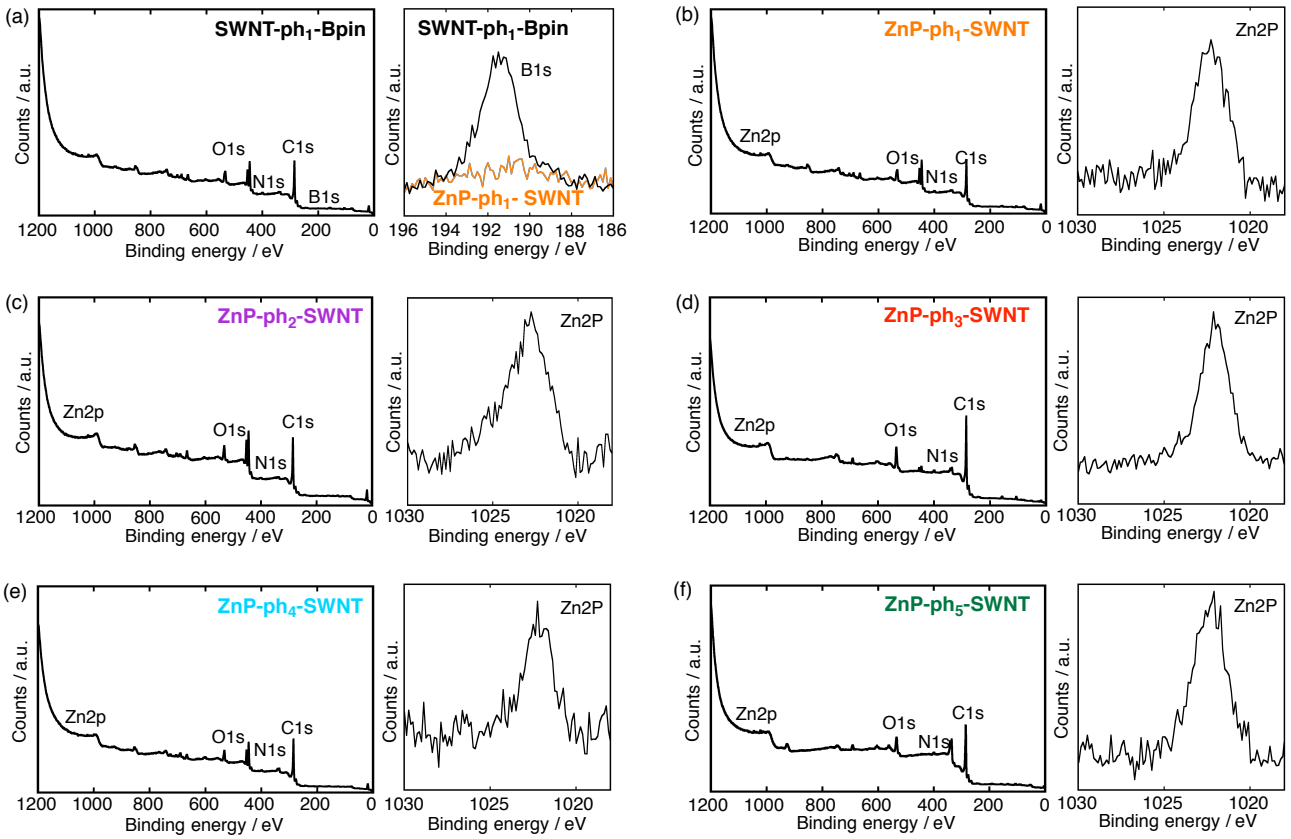

Figure S1. (a) XPS survey scan (left) and high-resolution XPS B1s spectrum (right) of SWNT-ph$_1$-Bpin (black line) and ZnP-ph$_1$-SWNT (orange line) as a typical spectrum of ZnP-ph$_n$-SWNT. The ratio of C/B was estimated to be 47, corresponding to a one phenylpinacolborane group per 35 carbon atoms of SWNT. XPS survey scans (left) and high-resolution XPS Zn2p spectra (right) of (b) ZnP-ph$_1$-SWNT, (c) ZnP-ph$_2$-SWNT, (d) ZnP-ph$_3$-SWNT, (e) ZnP-ph$_4$-SWNT, and (f) ZnP-ph$_5$-SWNT. The ratios of C/Zn were determined to be (b) 356, (c) 370, (d) 381, (e) 415, and (f) 421, corresponding to one porphyrin group per (b) 250, (c) 258, (d) 262, (e) 284, and (f) 284 carbon atoms of SWNT.

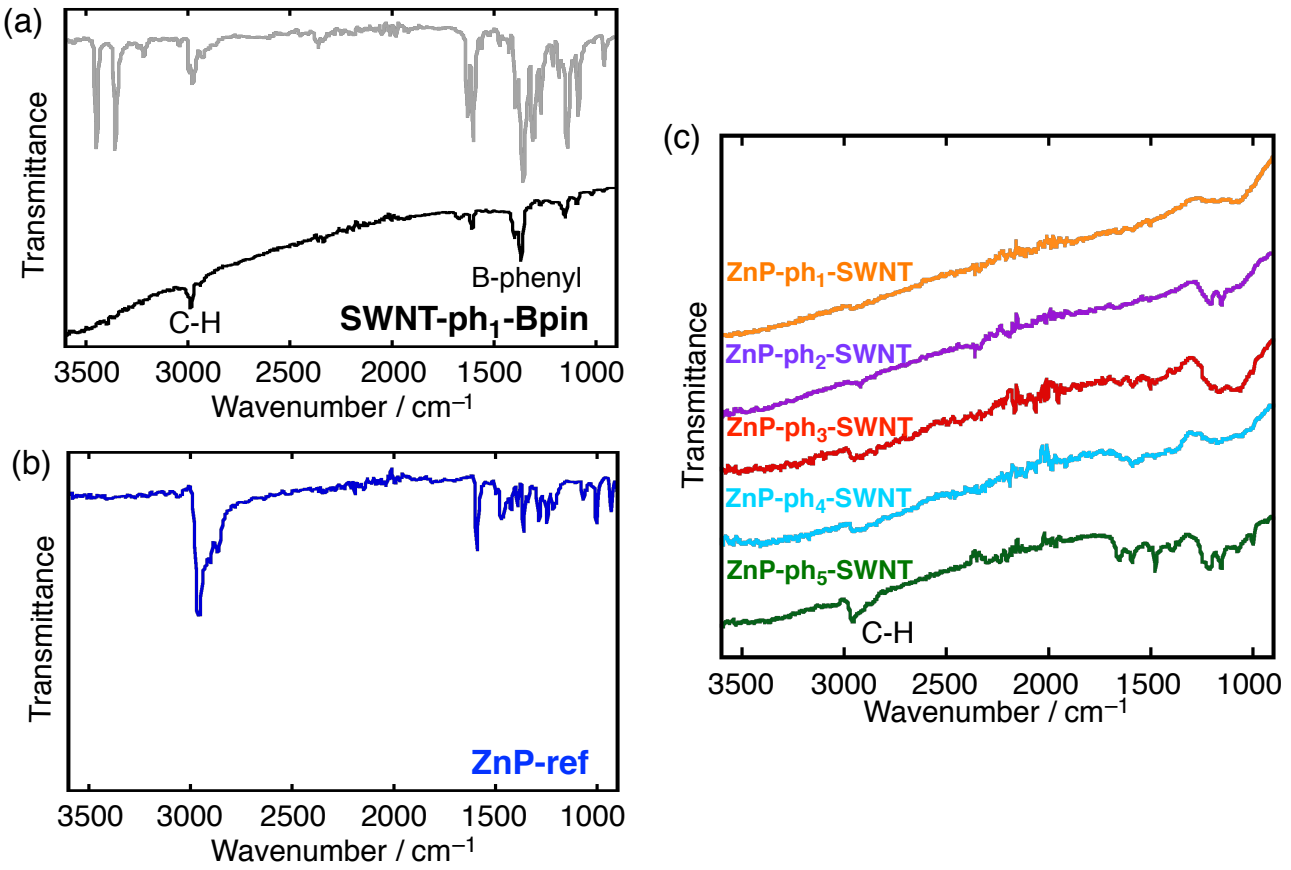

Figure S2. ATR-FTIR spectra of (a) 4-aminophenylboronic acid pinacol ester (gray line) and SWNT-ph$_1$-Bpin (black line), (b) ZnP-ref and (c) ZnP-ph$_n$-SWNT (n = 1–5). In panel (c), the normalized spectra are shown in parallel for comparison. A peak around 2960 cm^{-1} in the spectrum of ZnP-ph$_1$-SWNT (panel (c), orange line) is not obvious compared to that of SWNT-ph$_1$-Bpin (panel (a), black line) due to the lower functionalization ratio of ZnP group in ZnP-ph$_1$-SWNT than that of Bpin group in SWNT-ph$_1$-Bpin. The peak intensity around 2960 cm^{-1} in ZnP-ph$_n$-SWNT (n = 1–5) becomes larger with increasing the bridge length (panel (c)). It is known that the SWNT diminishes IR absorption intensities of molecules near the SWNT surface.[S5]

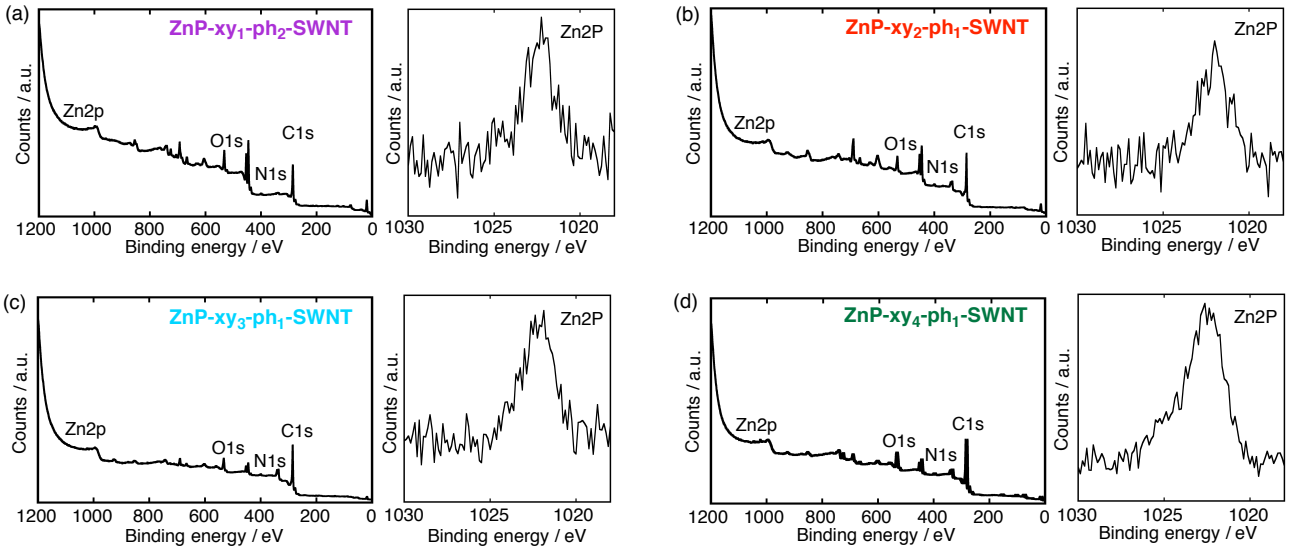

Figure S3. XPS survey scans (left) and high-resolution XPS Zn2p spectra (right) of (a) ZnP-xy_1-ph_1-SWNT, (b) ZnP-xy_2-ph_1-SWNT, (c) ZnP-xy_3-ph_1-SWNT and (d) ZnP-xy_4-ph_1-SWNT. The ratios of C/Zn were (a) 420, (b) 406, (c) 396 and (d) 429, corresponding to one porphyrin group per (a) 299, (b) 280, (c) 264, and (d) 286 carbon atoms of SWNT.

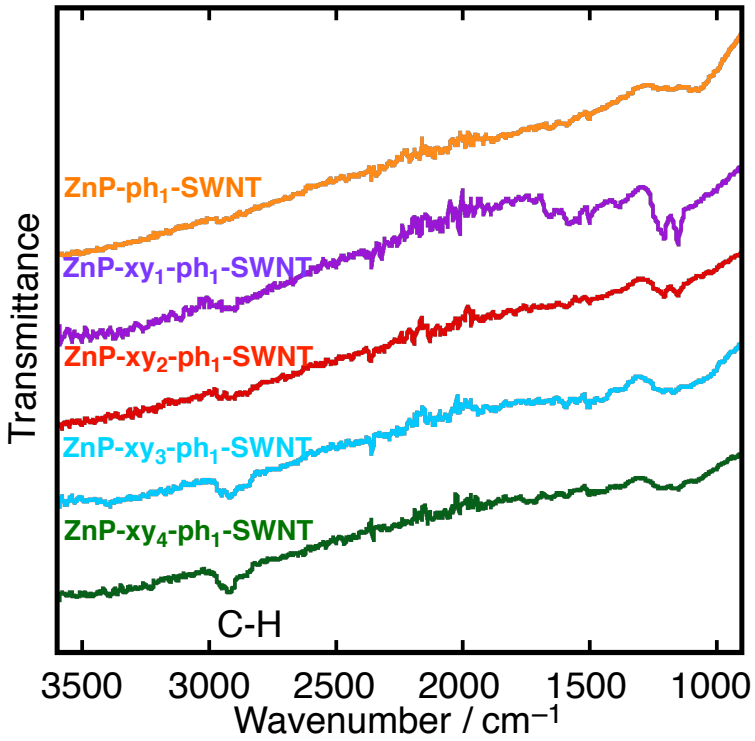

Figure S4. ATR-FTIR spectra of ZnP-xy$_{n-1}$-ph$_1$-SWNT (n = 1–5). The normalized spectra are shown in parallel for comparison.

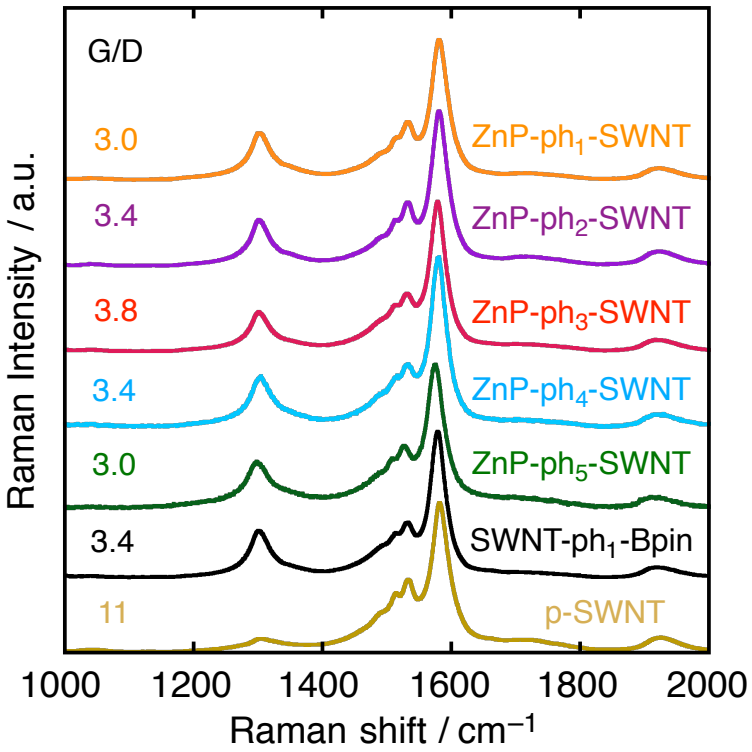

Figure S5. Resonant Raman spectra of p-SWNT, SWNT-ph$_1$-Bpin and ZnP-ph$_n$-SWNT (n = 1–5) with the excitation wavelength of 532 nm. The relative peak intensities of tangential mode (G-band) around 1600 cm^{-1} and of disorder mode (D-band) around 1350 cm^{-1} (G/D ratio) reflect the relative amounts of sp^3 carbon, and are used to determine the degree of sidewall functionalization.[S6] The G/D ratios of functionalized SWNTs (SWNT-ph$_1$-Bpin and ZnP-ph$_n$-SWNT) (3.0−3.8) are much smaller than that of purified-SWNT (11), which is reasonable considering that the phenylpinacolborane functionalization increases the defect sites on the sidewall of SWNT. On the other hand, the G/D ratios after the second functionalization showed no significant change (3.4 for SWNT-ph$_1$-Bpin and 3.0−3.8 for ZnP-ph$_n$-SWNT, respectively) because the Suzuki coupling reaction did not increase defect sites in the sp^2-hybridized SWNT domains.

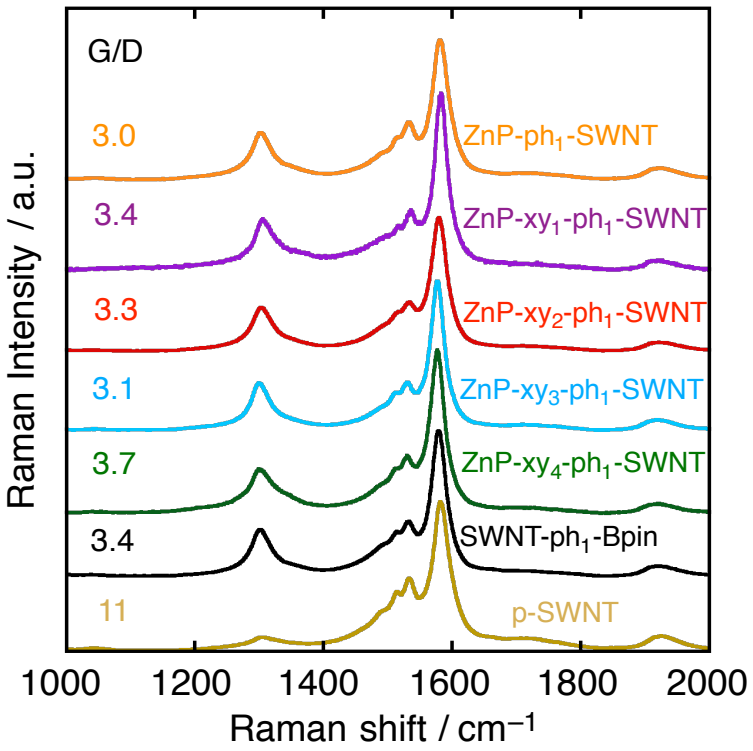

Figure S6. Resonant Raman spectra of p-SWNT, SWNT-ph_1-Bpin and ZnP-xy_{n-1}-ph_1-SWNT (n = 1–5) with the excitation wavelength of 532 nm. The G/D ratios of respective SWNTs are given in figure.

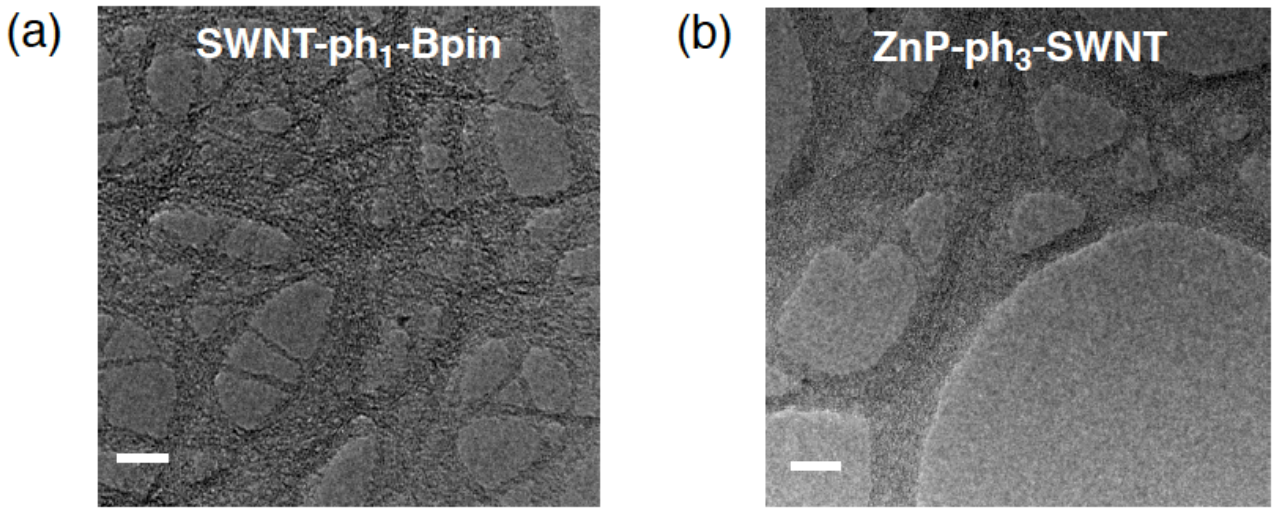

Figure S7. TEM images of (a) SWNT-ph_1-Bpin and (b) ZnP-ph_3-SWNT (scale bar: 10 nm). The samples were prepared by casting the DMF dispersion onto a carbon microgrid. The image of ZnP-ph_3-SWNT is shown as a typical example of the porphyrin-linked SWNTs.

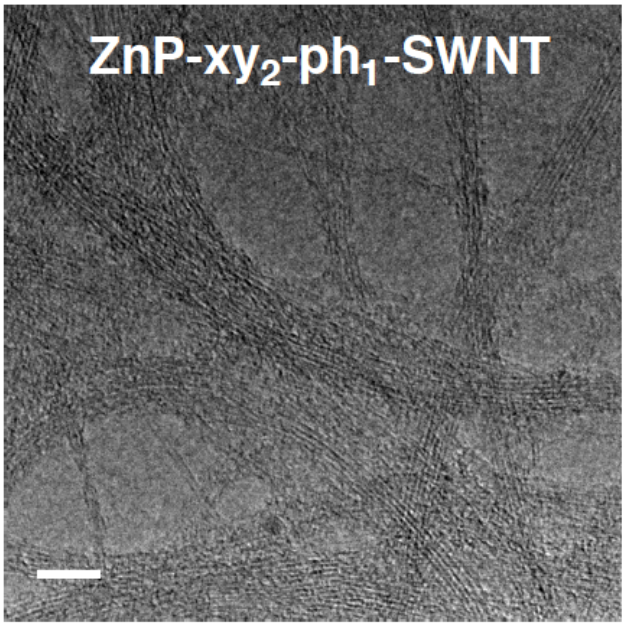

Figure S8. TEM image of ZnP-xy_2-ph_1-SWNT (scale bar: 10 nm). The sample was prepared by casting the DMF dispersion onto a carbon microgrid. The image of ZnP-xy_2-ph_1-SWNT is shown as a typical example of the porphyrin-linked SWNTs.

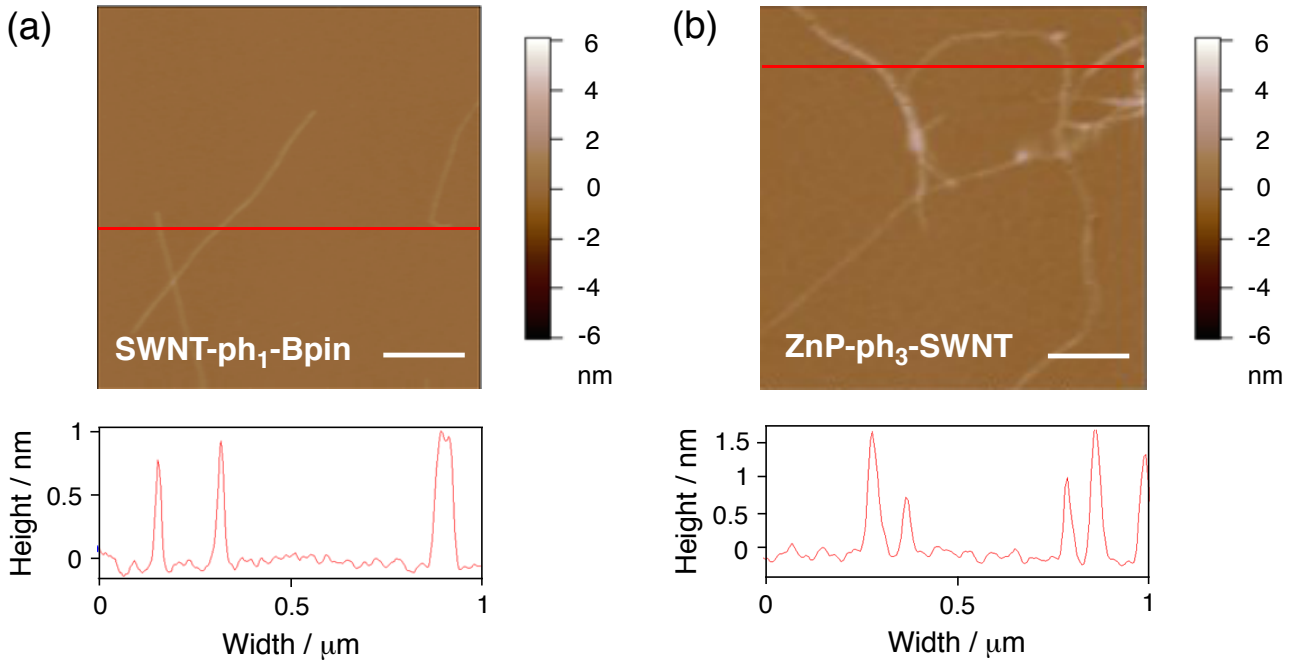

Figure S9. AFM images of (a) SWNT-ph$_1$-Bpin and (b) ZnP-ph$_3$-SWNT (scale bar: 200 nm). The samples were prepared by spin-coating the DMF dispersion on a freshly cleaved mica. The color scale represents the height topography, with light and dark representing the highest and lowest features, respectively. The image of ZnP-ph$_3$-SWNT is shown as a typical example of the porphyrin-linked SWNTs.

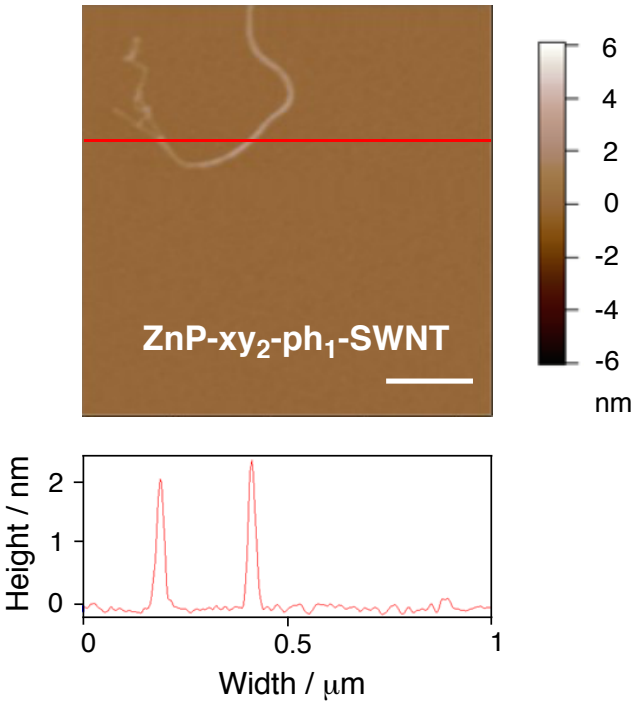

Figure S10. AFM image of ZnP-xy_2-ph_1-SWNT (scale bar: 200 nm). The sample was prepared by spin-coating the DMF dispersion on a freshly cleaved mica. The color scale represents the height topography, with light and dark representing the highest and lowest features, respectively. The image of ZnP-xy_2-ph_1-SWNT is shown as a typical example of the porphyrin-linked SWNTs.

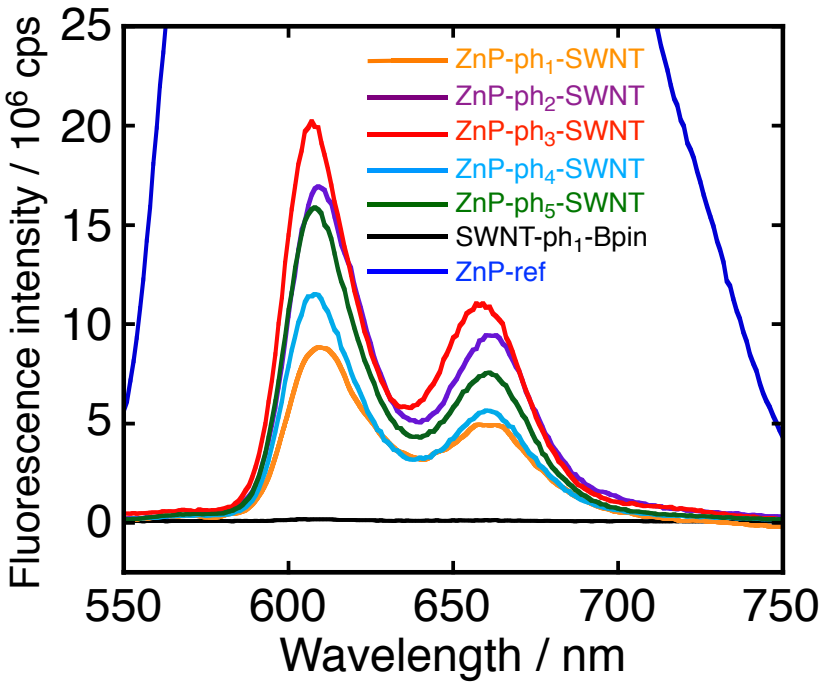

Figure S11. Enlarged steady-state fluorescence spectra (Figure 1b) of ZnP-ph$_1$-SWNT (orange), ZnP-ph$_2$-SWNT (purple), ZnP-ph$_3$-SWNT (red), ZnP-ph$_4$-SWNT (cyan), ZnP-ph$_5$-SWNT (green), SWNT-ph$_1$-Bpin (black), ZnP-ref (navy, 0.7 μM). For the excitations, the absorbances of the porphyrin moieties were adjusted to be identical at the peak position of the Soret band for comparison. While the quenching ratios of porphyrin fluorescence in all ZnP-ph$_n$-SWNT (n = 1−5) are remarkably high (> 98%), there is no clear relationship between the fluorescence intensities and the spacer lengths. The intensities of the porphyrin emissions in ZnP-ph$_n$-SWNT (n = 1−5) may bear relevance to the ratio of ZnP moieties linked at the edges and defect sites of SWNTs.

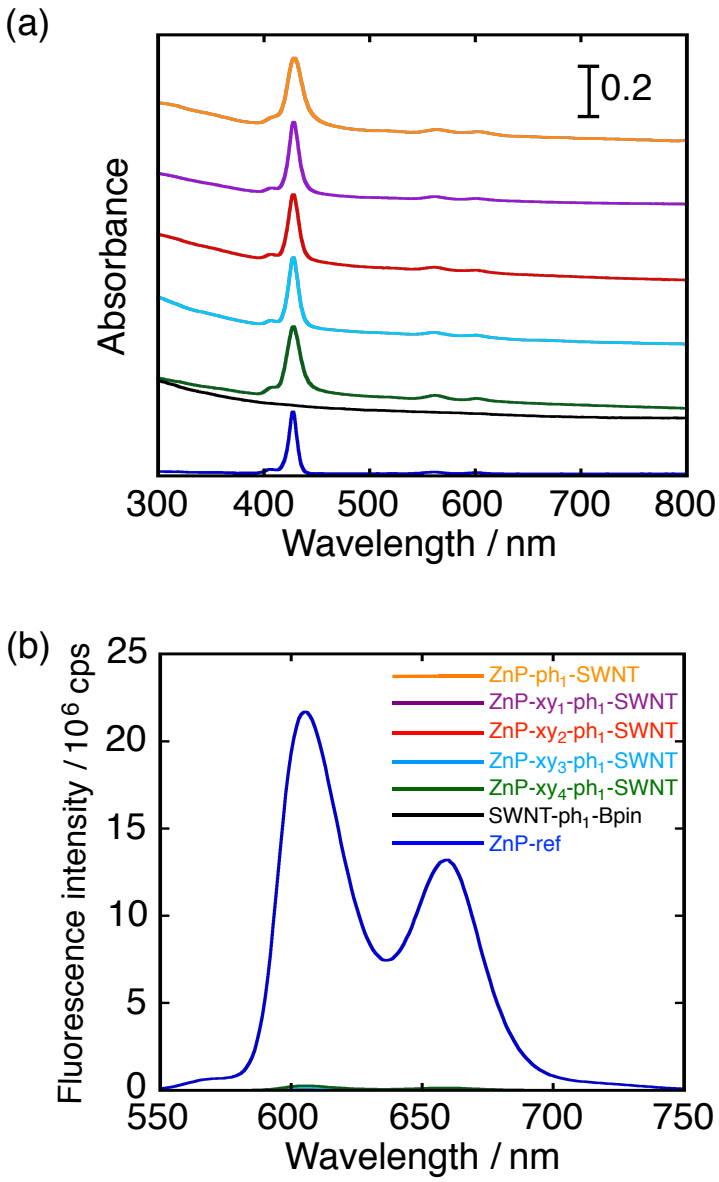

Figure S12. (a) Steady-state UV-visible absorption and (b) steady-state fluorescence spectra of ZnP-ph_1-SWNT (orange), ZnP-xy_1-ph_1-SWNT (purple), ZnP-xy_2-ph_1-SWNT (red), ZnP-xy_3-ph_1-SWNT (cyan), ZnP-xy_4-ph_1-SWNT (green), SWNT-ph_1-Bpin (black), and ZnP-ref (navy, 0.7 μM). The spectra in (a) are shown in parallel for comparison. For the excitations in (b), the absorbances of the porphyrin moieties were adjusted to be identical at the peak position of the Soret-band for comparison.

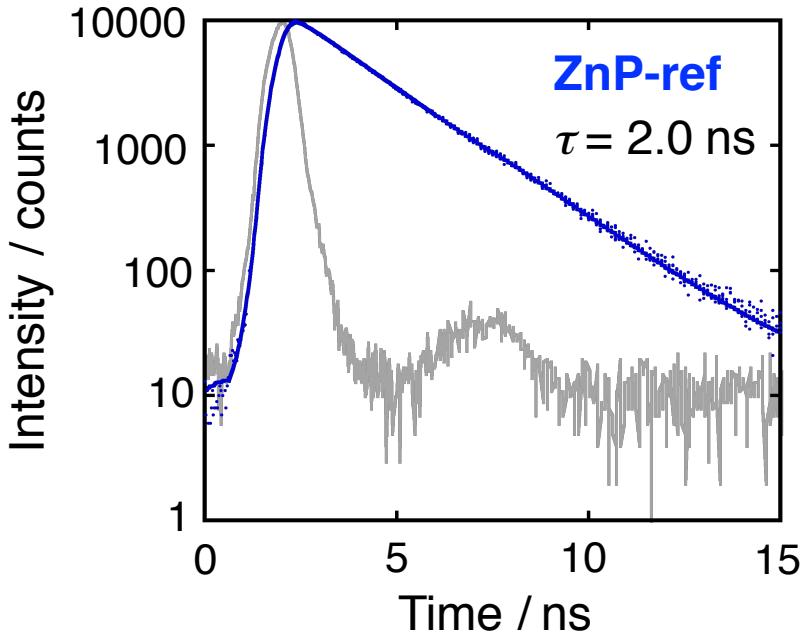

Figure S13. Fluorescence decay of ZnP-ref measured in DMF. The excitation and monitoring wavelengths are 430 and 610 nm, respectively. The solid blue line presents decay fitting and the gray line shows the instrumental response function. The fluorescence lifetime (τ) is given in the figure.

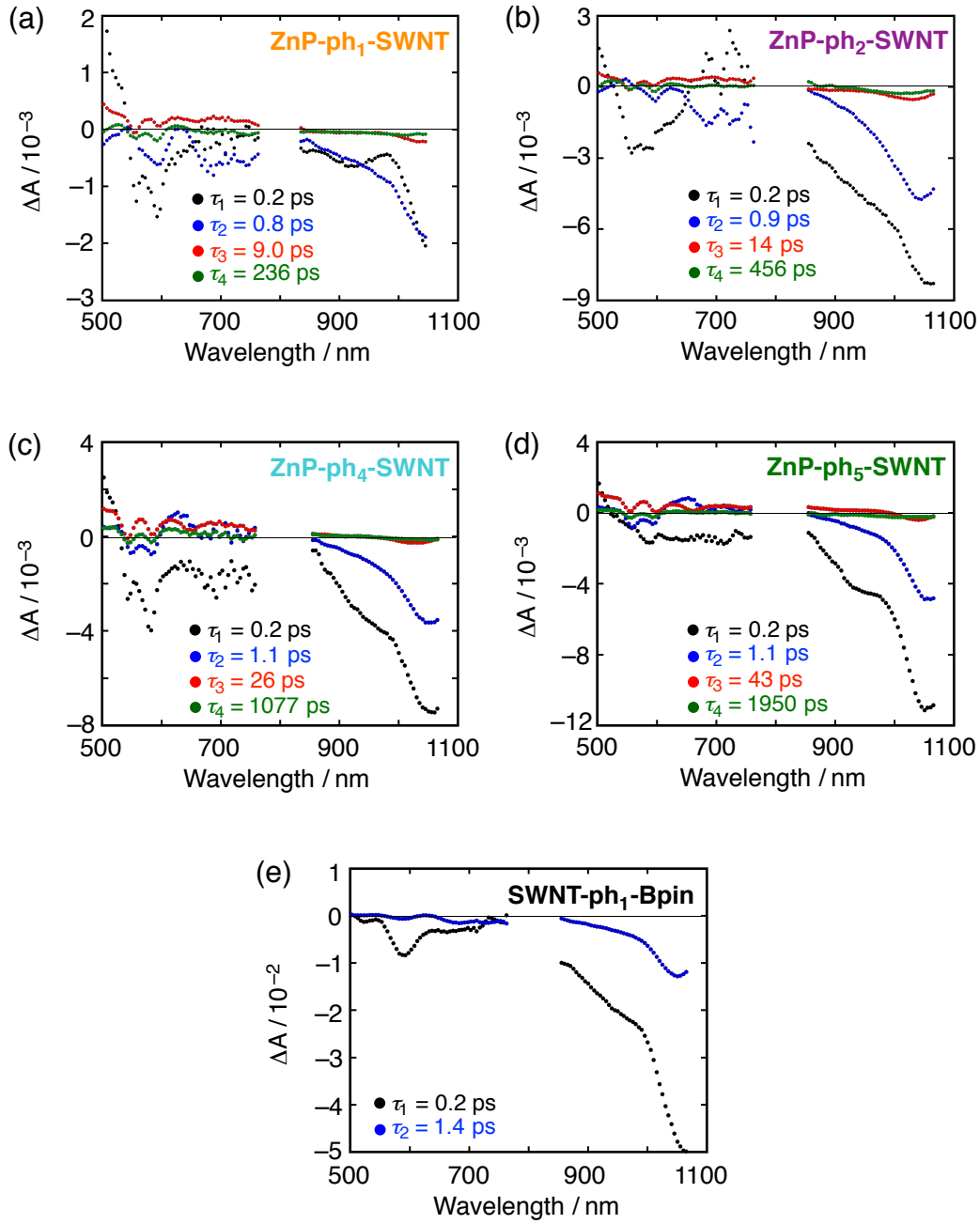

Figure S14. Transient absorption decay component spectra of (a) ZnP-ph$_1$-SWNT, (b) ZnP-ph$_2$-SWNT, (c) ZnP-ph$_4$-SWNT, and (d) ZnP-ph$_5$-SWNT in DMF obtained with global four component fit of the data, and (e) SWNT-ph$_1$-Bpin in DMF obtained with global two components fit of the data. The excitation wavelength is 430 nm. Lifetimes of respective components are given in the figures.

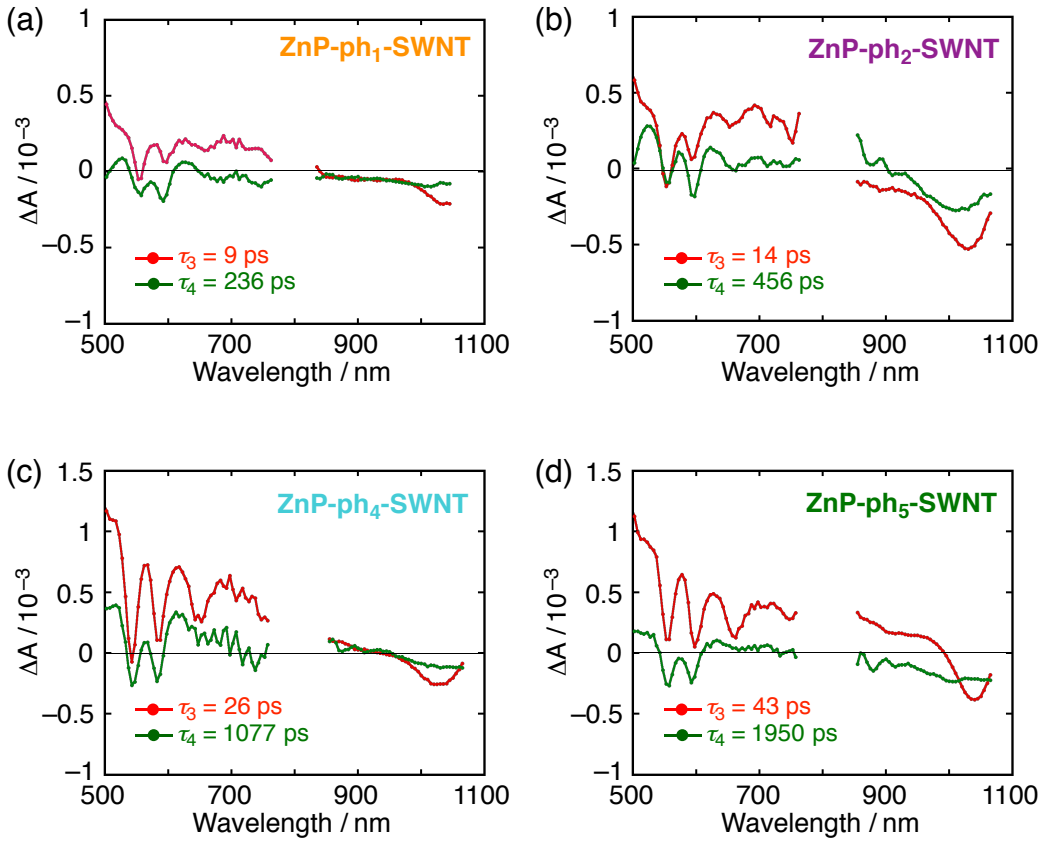

Figure S15. Enlarged transient absorption decay component spectra of (a) ZnP-ph$_1$-SWNT, (b) ZnP-ph$_2$-SWNT, (c) ZnP-ph$_4$-SWNT, and (d) ZnP-ph$_5$-SWNT in DMF obtained with global four component fit of the data. Only the third and fourth components are shown. The excitation wavelength is 430 nm. Lifetimes of respective components are given in the figures.

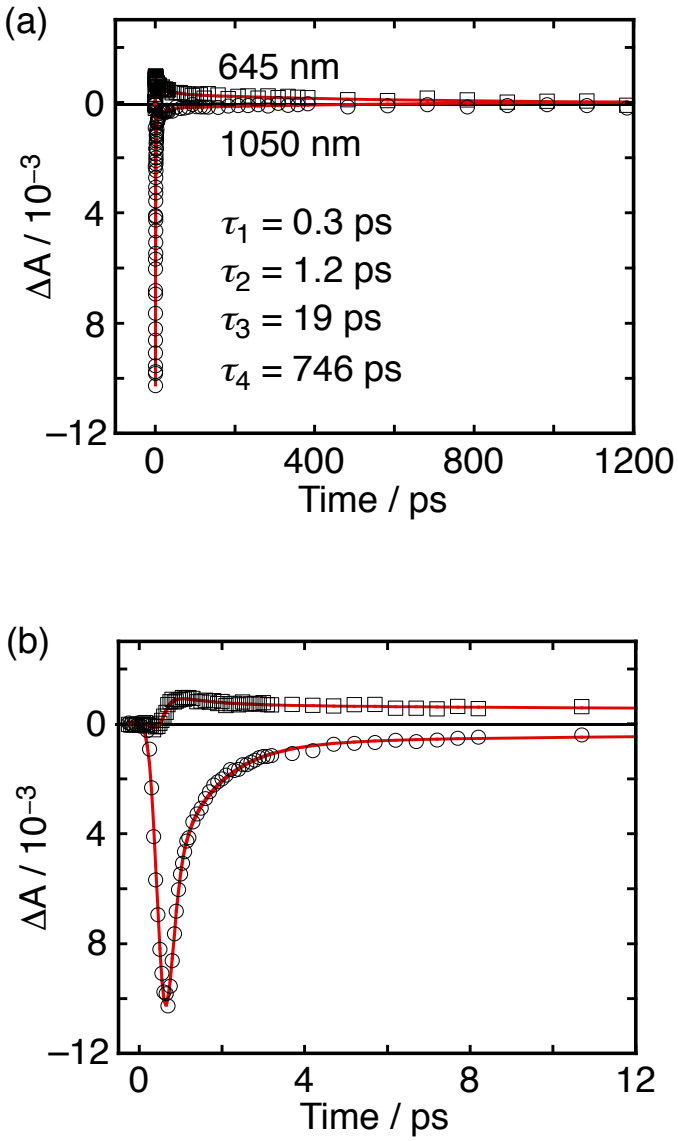

Figure S16 (a) Time traces of transient absorption signals of ZnP-ph$_3$-SWNT (Figure 3) detected at 645 (square) and 1050 nm (circle). (b) Enlarged spectra of (a). Solid red lines represent the results of tetra-exponential fitting obtained in Figure 3 and the lifetimes (τ) are given in the figure. The obtained fitting lines are coincided with the time traces of transient signals.

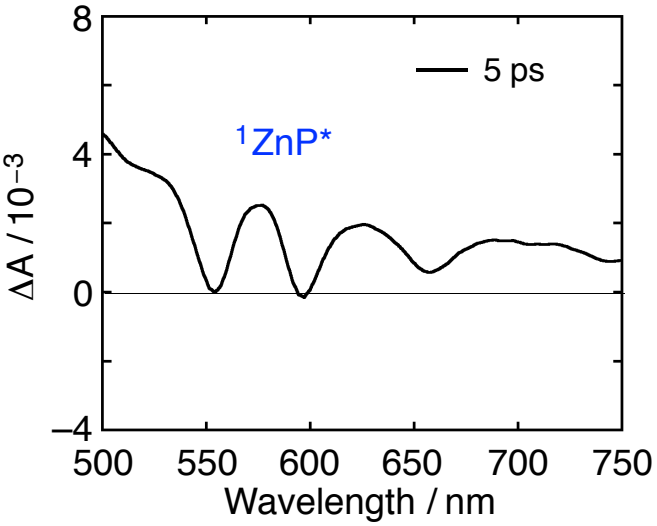

Figure S17. Time-resolved transient absorption spectra of ZnP-ref in DMF. The excitation wavelength is 430 nm. The time delay is 5 ps and the spectrum corresponds to the singlet excited-state of ZnP-ref (^{1}ZnP*).

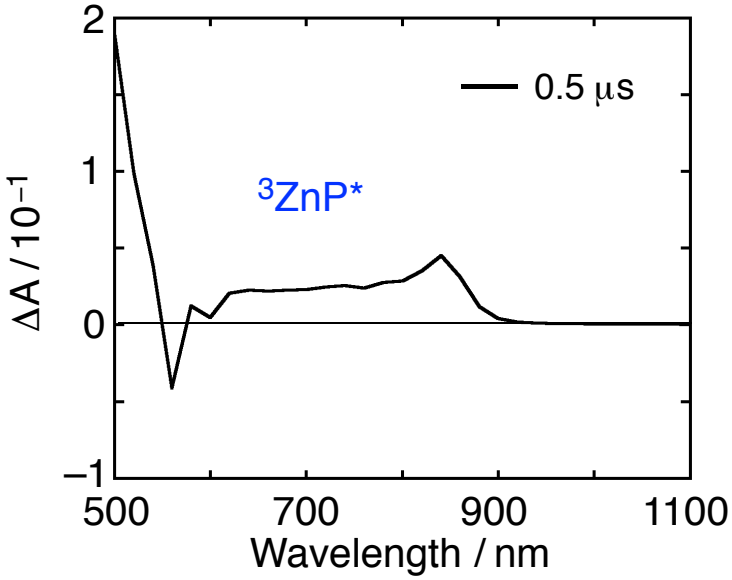

Figure S18. Time-resolved transient absorption spectra of ZnP-ref in benzonitrile. The excitation wavelength is 410 nm. The time delay is 0.5 μs and thereby the spectrum corresponds to the triplet excited-state of ZnP-ref (^{3}ZnP*).

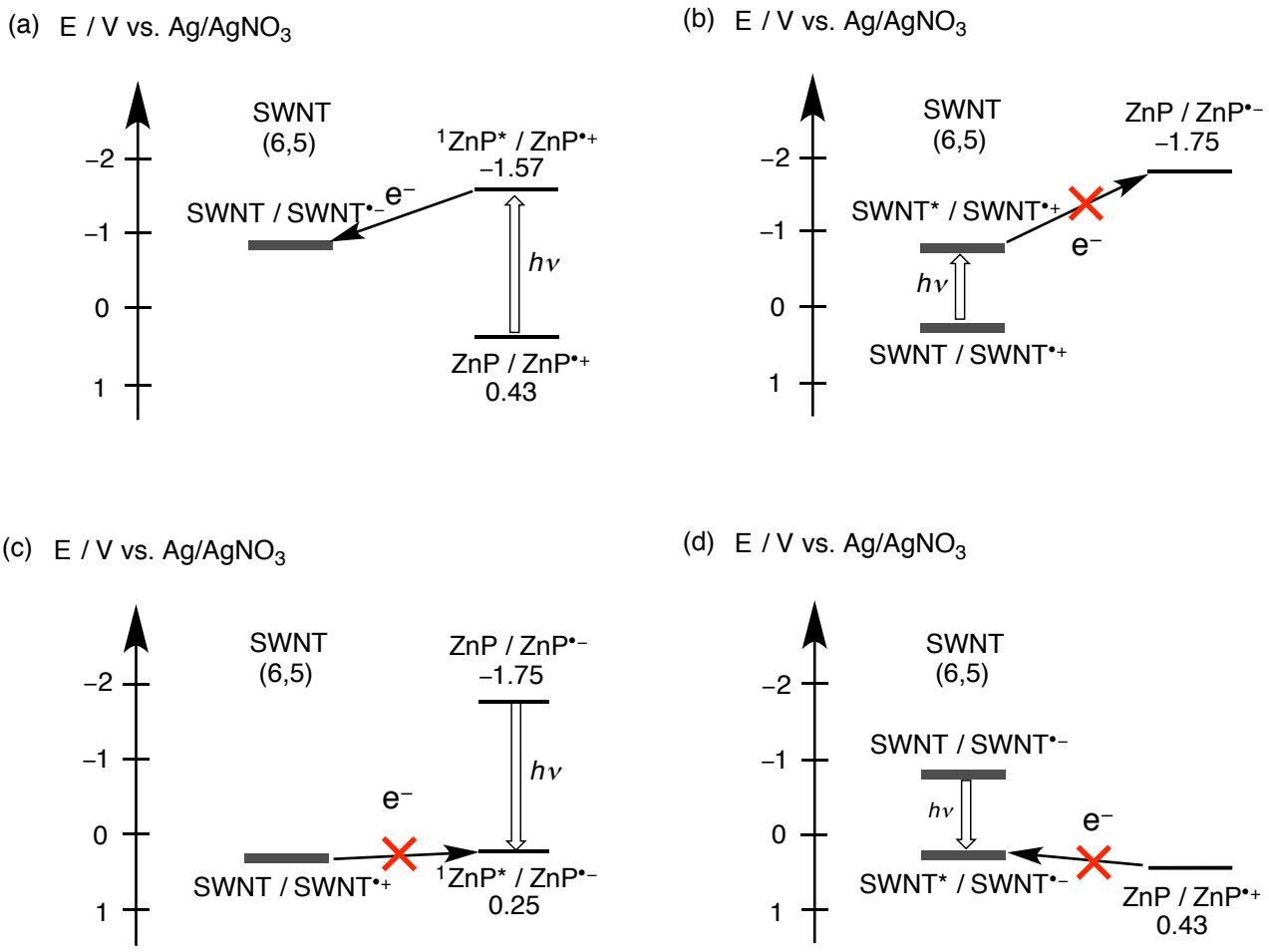

Figure S19. Energy diagrams for electron transfers (a) from the excited ^{1}ZnP* to SWNT, (b) from the excited SWNT* to ZnP, (c) from SWNT to the excited ^{1}ZnP*, and (d) from ZnP to the excited SWNT*. Redox potentials of ZnP were determined by cyclic voltammetry and differential pulse voltammetry measurements of ZnP-ref. The optical bandgap of ZnP was determined from the intersection point of the absorption and fluorescence spectra of ZnP-ref. The energy levels of redox potential and optical bandgap of the SWNT are taken from the literatures.[S7,S8] The process (a) is energetically favorable, but the other processes (b)−(d) are energetically unfavorable.

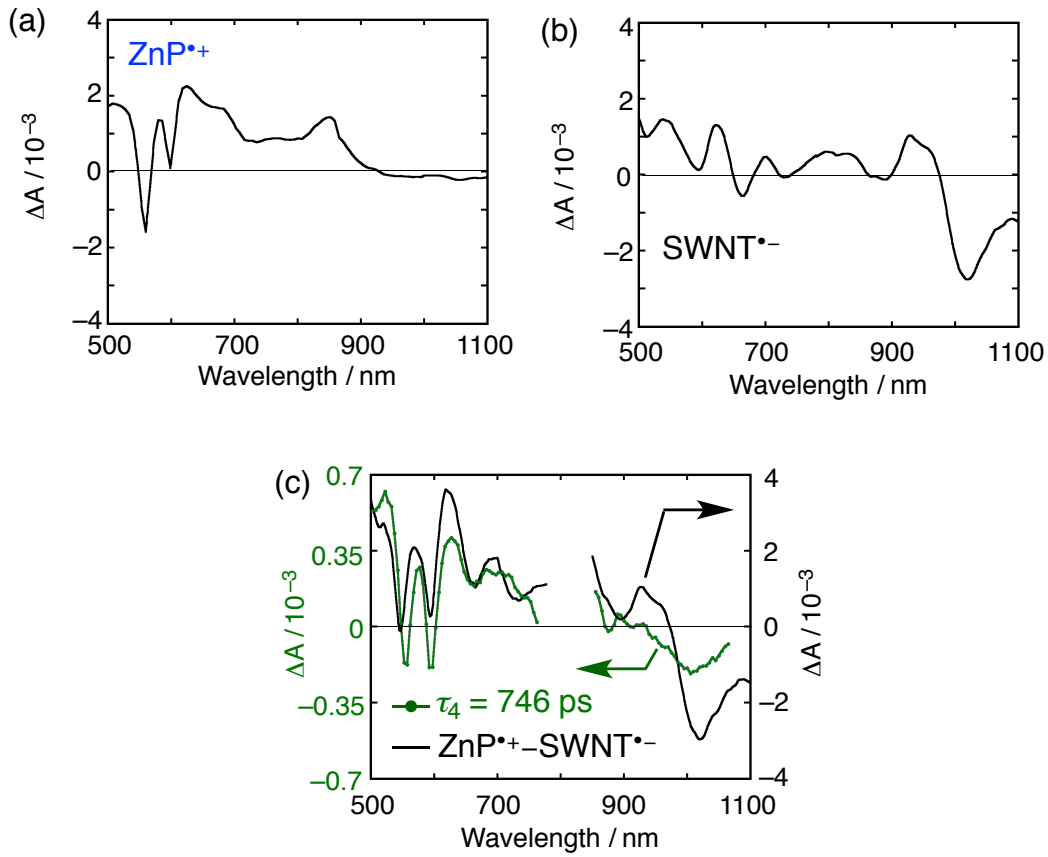

Figure S20. Differential absorption (ΔA) spectra of (a) ZnP-ref electrochemically oxidized at +1.1 V vs. $Ag/AgNO_3$ to generate the $ZnP^{\bullet+}$ and (b) p-SWNT electrochemically reduced at −1.4 V vs. $Ag/AgNO_3$ to generate the $SWNT^{\bullet-}$ in DMF using Bu_4NPF_6 (20 mM) as an electrolyte. The reference spectra correspond to the absorption spectra recorded in the absence of the applied potential. (c) Sum of the differential absorption (ΔA) spectra of the oxidized ZnP-ref ($ZnP^{\bullet+}$) and the reduced p-SWNT ($SWNT^{\bullet-}$) without the region of 770−850 nm. The fourth decay component spectrum in Figure 3 is also represented for comparison.

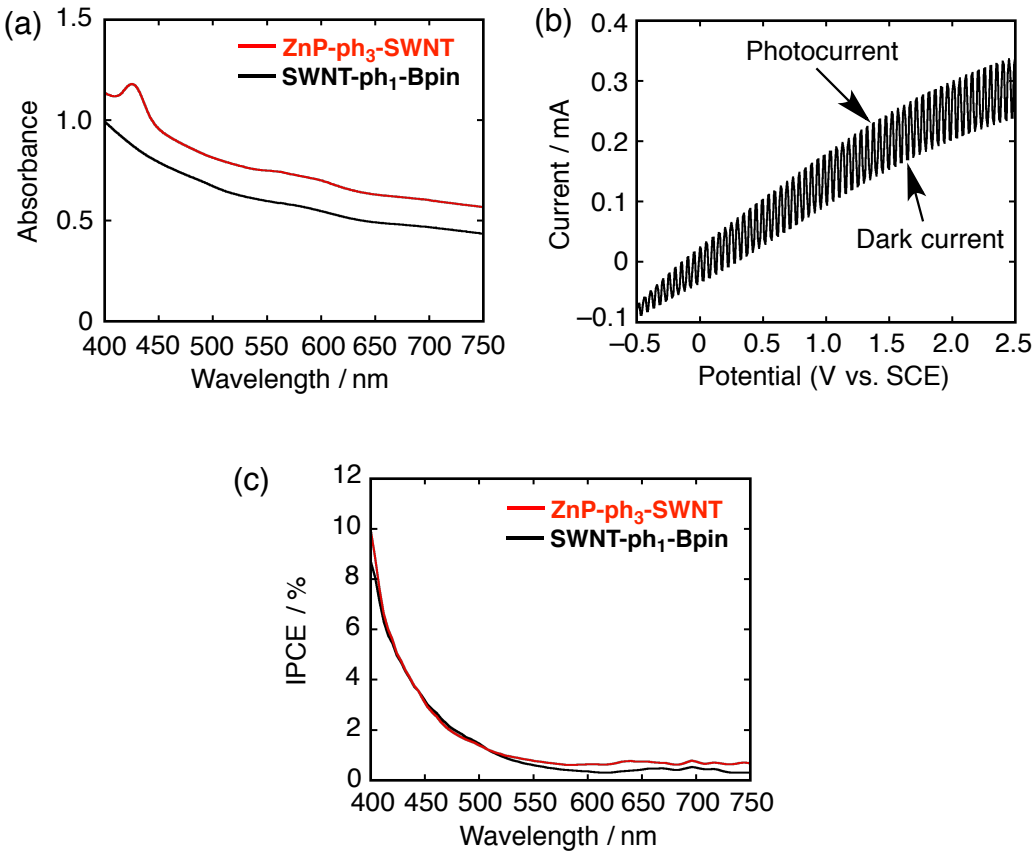

Figure S21. (a) Steady-state UV-vis absorption spectra of FTO/SnO_2/ZnP-ph_3-SWNT (red line) and FTO/SnO_2/SWNT-ph_1-Bpin electrodes (black line). The FTO/SnO_2/SWNT-ph_1-Bpin electrode exhibited featureless SWNT absorption that decreased monotonically from the UV to the NIR regions, whereas the FTO/SnO_2/ZnP-ph_3-SWNT electrode revealed the characteristic absorption due to the porphyrin moieties together with the SWNT absorption. (b) Current vs. potential curve for the FTO/SnO_2/ZnP-ph_3-SWNT device. Illuminated with white light (λ > 380 nm, input power: 35 mW cm^{-2}). Electrolyte: 0.5 M LiI and 0.01 M I_2 in acetonitrile. With increasing positive bias up to 0.175 V vs SCE, the photocurrent increased compared to the dark conditions current. Therefore, the IPCE values were compared at an applied potential of 0.175 V vs. SCE. (c) Photocurrent action spectra of the FTO/SnO_2/ZnP-ph_3-SWNT (red line) and FTO/SnO_2/SWNT-ph_1-Bpin (black line) devices. Applied potential: 0.175 V versus SCE; electrolyte: 0.5 M LiI and 0.01 M I_2 in acetonitrile.

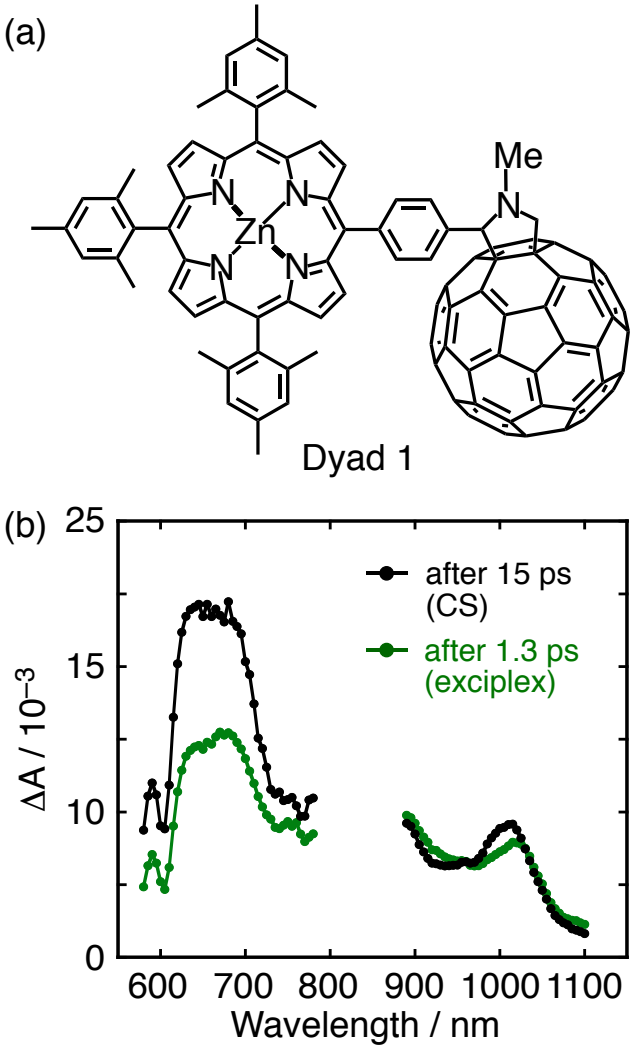

Figure S22. (a) Structure and (b) time-resolved spectra of Dyad 1 in benzonitrile with the excitation wavelength of 560 nm, which were already reported by Tkachenko et al.[S9] The photoexcitation of Dyad 1 yielded the charge-separated state via the exciplex state as an intermediate.[S9] The spectrum of the exciplex state (after 1.3 ps) resembles that of complete charge-separated state (after 15 ps) in shape, but significantly different in intensity.

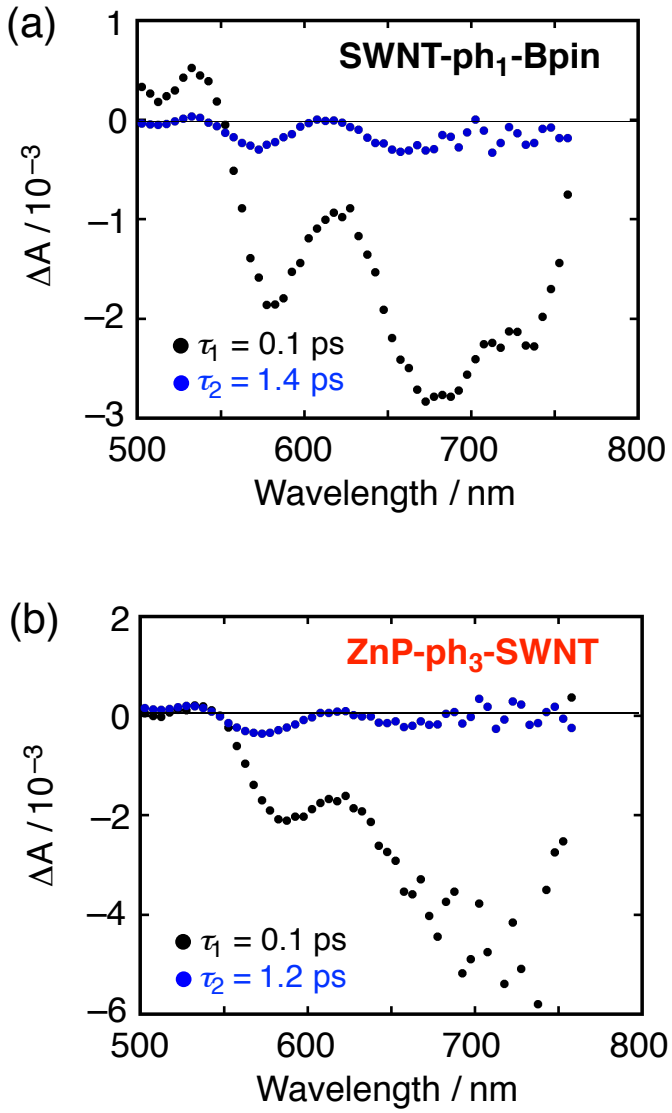

Figure S23. Transient absorption decay component spectra of (a) SWNT-ph_1-Bpin and (b) ZnP-ph_3-SWNT excited at the first interband transition of semiconducting-SWNT (S_{11}) (1030 nm) in DMF and obtained with global two components fit of the data. Lifetimes of respective components are given in the figures.

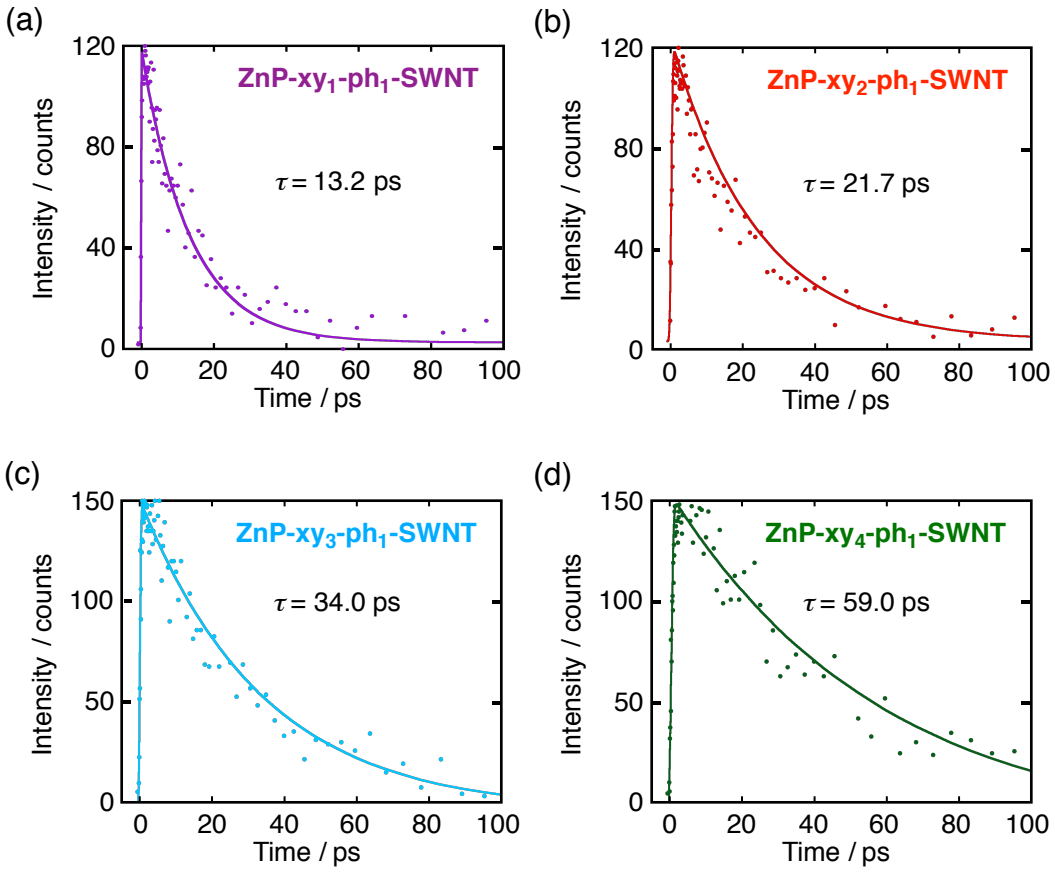

Figure S24. Fluorescence decays of (a) ZnP-xy$_1$-ph$_1$-SWNT, (b) ZnP-xy$_2$-ph$_1$-SWNT, (c) ZnP-xy$_3$-ph$_1$-SWNT and (d) ZnP-xy$_4$-ph$_1$-SWNT measured in DMF by a photon up-conversion technique. The excitation and detection wavelengths are 425 and 610 nm, respectively. The solid lines present decay fittings and the fluorescence lifetimes (τ) are given in the figures.

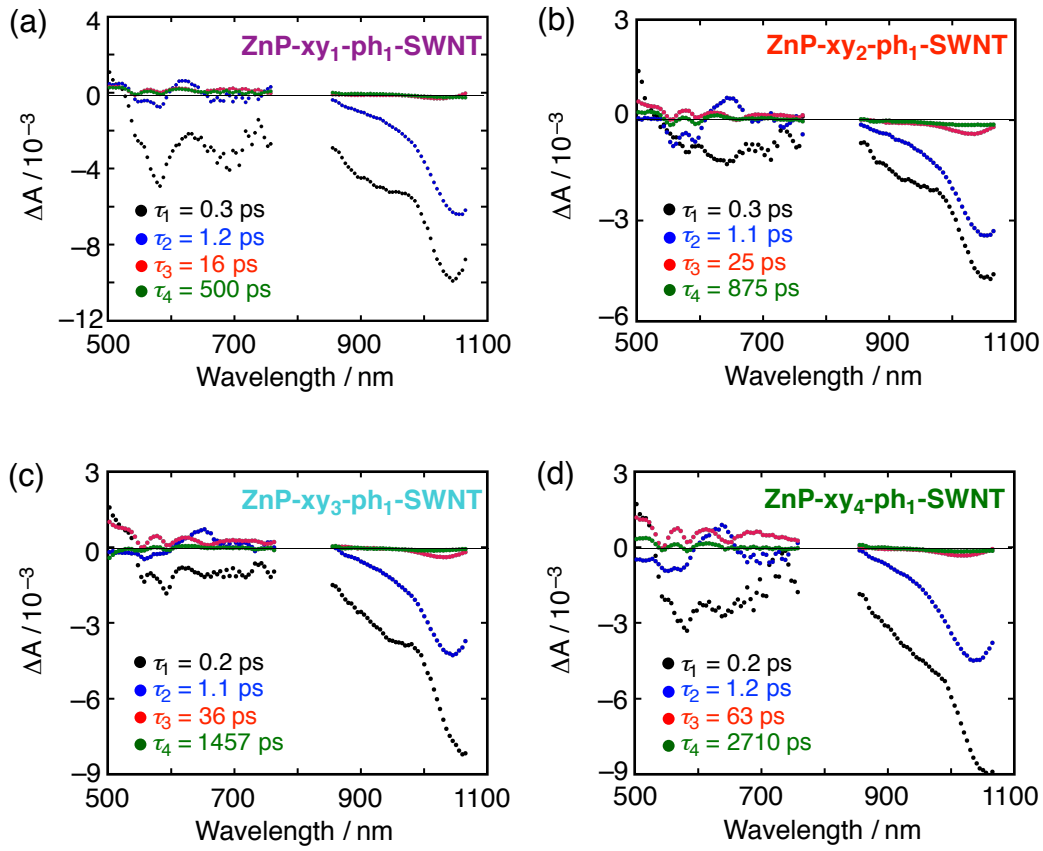

Figure S25. Transient absorption decay component spectra of (a) ZnP-xy$_1$-ph$_1$-SWNT, (b) ZnP-xy$_2$-ph$_1$-SWNT, (c) ZnP-xy$_3$-ph$_1$-SWNT, and (d) ZnP-xy$_4$-ph$_1$-SWNT in DMF obtained with global four components fit of the data. The excitation wavelength is 430 nm. Lifetimes of respective components are given in the figures.

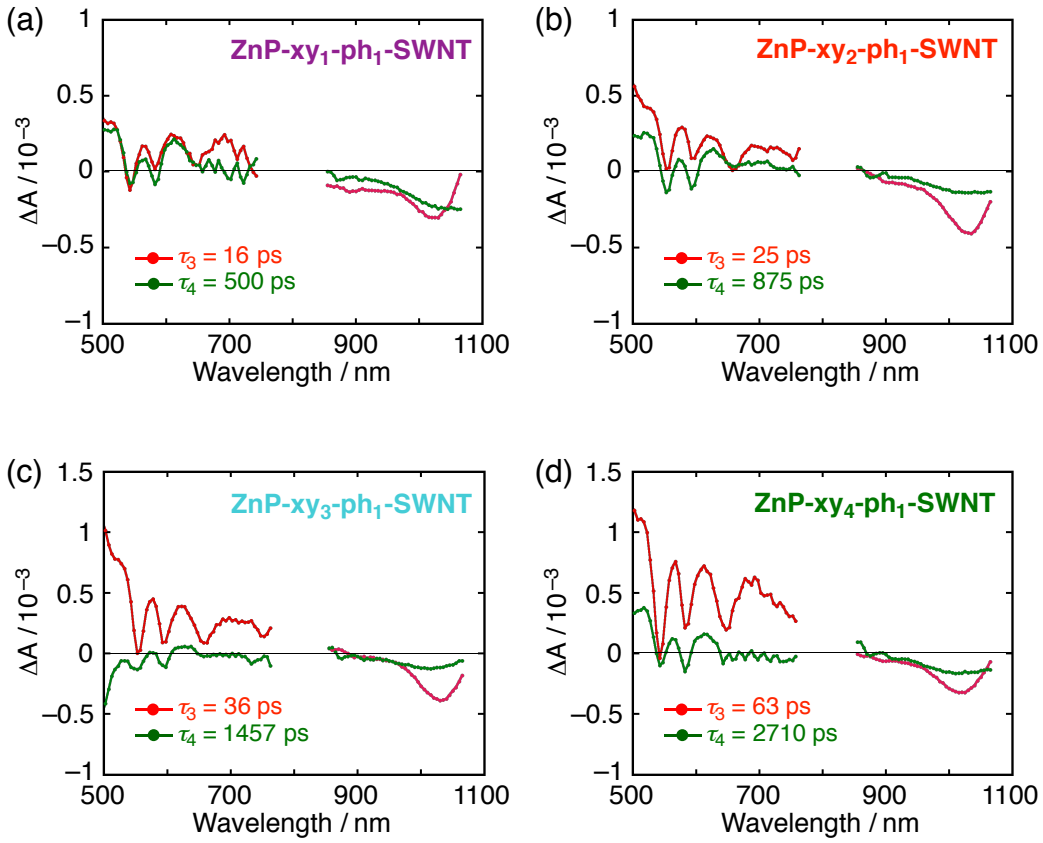

Figure S26. Enlarged transient absorption decay component spectra of (a) ZnP-xy$_1$-ph$_1$-SWNT, (b) ZnP-xy$_2$-ph$_1$-SWNT, (c) ZnP-xy$_3$-ph$_1$-SWNT, and (d) ZnP-xy$_4$-ph$_1$-SWNT in DMF obtained with global four component fit of the data. Only the third and fourth components are shown. The excitation wavelength is 430 nm. Lifetimes of respective components are given in the figures.

References in Supporting Information

[S1] Umeyama, T.; Mihara, J.; Tezuka, N.; Matano, Y.; Stranius, K.; Chukharev, V.; Tkachenko, N. V.; Lemmetyinen, H.; Noda, K.; Matsushige, K.; Shishido, T.; Liu, Z.; Hirose-Takai, K.; Suenaga, K.; Imahori, H. *Chem. Eur. J.* **2012**, *18*, 4250−4257.

[S2] Frampton, M. J.; Akdas, H.; Cowley, A. R.; Rogers, J. E.; Slagle, J. E.; Fleitz, P. A.; Drobizhev, M.; Rebane, A.; Anderson, H. L. *Org. Lett.* **2005**, *7*, 5365–5368.

[S3] Grunder, S.; Valente, C.; Whalley, A. C.; Sampath, S.; Portmann, J.; Botros, Y. Y.; Stoddart, J. F. *Chem. Eur. J.* **2012**, *18*, 15632−15649.

[S4] Ousaka, N.; Grunder, S.; Castilla, A. M.; Whalley, A. C.; Stoddart, J. F.; Nitschke, J. R. *J. Am. Chem. Soc.* **2012**, *134*, 15528−15537.

[S5] Setyowati, K.; Piao, M. J.; Chen, J.; Liu, H. *Appl. Phys. Lett.* **2008**, *92*, 043105.

[S6] Stephenson, J. J.; Hudson, J. L.; Azad, S.; Tour, J. M. *Chem. Mater.* **2006**, *18***,** 374−377.

[S7] Hirana, Y.; Juhasz, G.; Miyauchi, Y.; Mouri, S.; Matsuda, K.; Nakashima, N. *Sci. Rep.* **2013**, *3*, 2959.

[S8] Tanaka, Y.; Hirano, Y.; Niidome, Y.; Kato, K.; Saito, S.; Nakashima, N. *Angew. Chem. Int. Ed.* **2009**, *48*, 7655−7659.

[S9] Pelado, B.; Abou-Chahine, F.; Calbo, J.; Caballero, R.; de la Cruz, P.; Junquera-Hernández, J. M.; Ortí, E.; Tkachenko, N. V.; Langa, F. *Chem. Eur. J.* **2015**, *21*, 5814−5825.

References in the Main Text with Full List of Authors

[31] Ehli, C.; Rahman, G. M. A.; Jux, N.; Balbinot, D.; Guldi, D. M.; Paolucci, F.; Marcaccio, M.; Paolucci, D.; Melle-Franco, M.; Zerbetto, F.; Campidelli, S.; Prato, M. *J. Am. Chem. Soc.* **2006**, *128*, 11222–11231.

[35] Umeyama, T.; Mihara, J.; Hayashi, H.; Kadota, N.; Chukharev, V.; Tkachenko, N. V.; Lemmtyinen, H.; Yoshida, K.; Isoda, S.; Takano, M.; Imahori, H. *Chem. Commun.* **2011**, *47*, 11781–11783.

[45] Umeyama, T.; Mihara, J.; Tezuka, N.; Matano, Y.; Stranius, K.; Chukharev, V.; Tkachenko, N. V.; Lemmetyinen, H.; Noda, K.; Matsushige, K.; Shishido, T.; Liu, Z.; Hirose-Takai, K.; Suenaga, K.; Imahori, H. *Chem. Eur. J.* **2012**, *18*, 4250−4257.

[48] Kim, M.; Adamska, L.; Hartmann, N. F.; Kwon, H.; Liu, J.; Velizhanin, K. A.; Piao, Y.; Powell, L. R.; Meany, B.; Doorn, S. K.; Tretiak, S.; Wang, Y. *J. Phys. Chem. C* **2016**, *120*, 11268–11276.

[53] Umeyama, T.; Tezuka, N.; Kawashima, F.; Seki, S.; Matano, Y.; Nakao, Y.; Shishido, T.; Nishi, M.; Hirao, K.; Lehtivuori, H.; Tkachenko, N. V.; Lemmetyinen, H.; Imahori, H. *Angew. Chem. Int. Ed.* **2011**, *50*, 4615–4619.